annalen der physik
www.ann-phys.org

Suppression of the Stimulated Brillouin and Raman Scattering in Actively Q-switched Fiber Lasers through Temporal Pulse Shaping

Sina Jafari, Davood Fathi, Hussein Taleb, and Derek Abbott*

Despite the wide range of applications and versatility, actively Q-switched fiber lasers (AQS-FLs) suffer from the multi-peak phenomenon or stepwise pulse generation under certain conditions. As such, the advantage of the stepwise tendency in AQS-FL to modify the pulse shape and create a temporal profile that minimizes the power of stimulated Brillouin scattering (SBS) and stimulated Raman scattering (SRS) Stokes components is taken. Accordingly a multi-objective genetic algorithm (GA) and a Monte-Carlo method is developed to solve the improved model for SBS. Additionally, the suppression of SRS is predicted and examined successfully. The proposed method is deployed for the simulation of the 5 and 10 kW peak and 10 ns wide pulses on a 4 m long, single-mode, ytterbium-doped double clad fiber under the narrow linewidth of 0.05 nm with promising suppression of SBS and SRS effects. To the best of the authors' knowledge this is the first time that such a pulse-shaping strategy is demonstrated for the SBS or SRS suppression. Furthermore reaching a 10 kW peak on single mode fibers was previously only possible via custom made fibers. Our novel method offers the possibility of optimizing and improving the utilization of different fiber types in AQS-FL systems.

1. Introduction

The actively Q-switched fiber laser (AQS-FL) is a conventional choice for generating the nanosecond pulses. A single stage AQS-FL can be utilized as a high beam quality seed to the input of power amplifier stage in a master oscillator power amplifier (MOPA) configuration or as a direct laser source for material processing, scientific instrumentation, medical applications, ranging, etc. The gain switching (GS) concept on the other hand, can be explained via pump diode modulation[1,2]—this can be on/off switching or Gaussian modulation. Gain-switched fiber laser (GS-FL) concepts, design, modeling and applications are similar to that of the Q-switched type in many regards. The novel method and framework in this paper builds upon the presented theoretical background, improved numerical modeling, and simulations. Our novel method predicts that using the slope (pulse growth rate) optimization, it is possible to eliminate or very effectively suppress the unwanted stimulated Brillouin scattering (SBS) and stimulated Raman scattering (SRS) phenomena in AQS-FLs. To properly model and explain the different observed phenomena in AQS-FL systems, it is necessary to provide some details about their different operational aspects and contributing mechanisms, as follows.

Note that AQS-FLs offer a degree of flexibility and are partially controllable due to employing a type of optical Q-switch modulator, however, the chaotic behavior, perturbation, and time variance of the system make it difficult to generate predictable and regular pulse shapes under desired repetition regimes.[3–5] One of the undesired phenomena in an AQS-FL is the multi-peak phenomenon (MPP), shown in **Figure 1** from our rigorous numerical simulation results, which can be described by the system dynamics and the impact of SBS.[3,6] Note that MPP occurs when the modulator rise time is smaller than the cavity round trip time and in a less serious form shows itself as a stepwise temporal profile as is explained and experimentally shown in refs. [7, 8]. An AQS-FL system is always prone to such a condition, thus we exploit this stepwise tendency of AQS-FLs to create some small steps during the initial stages of pulse growth. This stepwise initial growth combined with proper exponential behavior can give rise to gain consumption or gain saturation dominating the main lasing process over the SBS/SRS Stokes processes that leads to effective SBS and SRS suppression—in other words, it can be said that some management of system energy storage/recovery is performed.

The difficulty of realizing this idea and method which has its roots in the complex behavior of the AQS-FLs, can be simplified by exploiting artificial intelligence (AI) algorithms such as the genetic algorithm (GA) to find an optimal, self-taught, and temporal

S. Jafari, Dr. D. Fathi, Dr. H. Taleb
Department of Electrical and Computer Engineering
Tarbiat Modares University (TMU)
Tehran 1411713116, Iran
E-mail: d.fathi@modares.ac.ir
Prof. D. Abbott
School of Electrical and Electronic Engineering
University of Adelaide
Adelaide, SA 5005, Australia

The ORCID identification number(s) for the author(s) of this article can be found under https://doi.org/10.1002/andp.202000541

DOI: 10.1002/andp.202000541

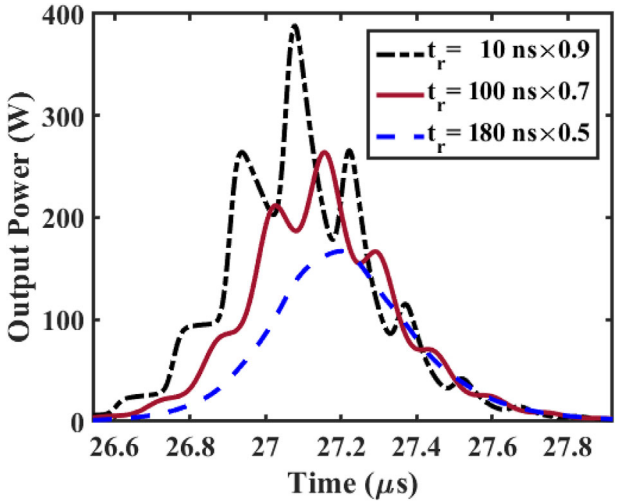

Figure 1. The multi-peak and stepwise phenomena and their dependence on the modulator rise time.

behavior for generating a proper pulse shape that excites the minimum Stokes power. We have already proposed and predicted in our previous work[9] that single and pulse train generation processes for the AQS-FL can be optimized and customized in an effective and feasible manner using GA. In this paper, we have considered a single stage, single transverse mode pulsed fiber laser, utilizing a large mode area (LMA) ytterbium-doped double clad fiber (YD-DCF) with the core/inner cladding diameters of 10/125 μm and featuring a combination of Q and gain switching techniques. A rigorous, detailed, wavelength dependent and transient model for SBS and SRS with some improvements over previous developed models is deployed that accounts for the interplay between the ASE and SBS–SRS processes. Stochastic SBS analysis is performed using one of the Monte–Carlo methods. A narrow lasing linewidth of 0.05 nm is assumed to demonstrate a worst-case scenario regarding SBS enhancement for narrow linewidth lasers.[10]

In order to highlight and clarify the framework and limitations of this research, it is necessary to mention that the practical peak power range for single mode AQS-FLs would be a few kilowatts[11,12] and usually their pulse width lies in the range of a few to hundreds of nanoseconds—higher peak powers fall into one of the following categories; multistage configuration (e.g. MOPA), specialty, rod type or custom (lab made) fibers, compressed pulse FLs, stochastic FLs, multi-transverse mode FLs, combined beam FLs or a combination of the above methods. This work concentrates on ordinary LMA fibers featuring reasonable cost, however the proposed method can be extended to other (above mentioned) classes of fibers,[13–15] the aim in any case is to maximize the fiber's utility, while minimizing cost and design time.

The paper is organized as follows. Section 2 is dedicated to the theoretical background and dynamics of the AQS-FL systems, gain switching concept and introduction to nonlinear scattering effects in fiber. In Section 3 we derive and improve a numerical model for the SBS analysis. Section 4 is dedicated to the numerical modeling of the SRS effect. In Section 5 we introduce our developed GA. Section 6 offers the details and values for the simulation parameters and setup. Finally, in Section 7 we discuss the SBS and SRS suppression results. Moreover, the feasibility and practicality of our proposed framework and method is discussed in this section.

2. Theoretical Background

The schematic of the proposed AQS-FL system is shown in **Figure 2**, in which a beam sampler installed on the system output reflecting a small percent of the beam to be detected by a photodetector (PD) and trigger a control (driver) circuit for the pump diode. The simple idea for gain switching is turning on and off the pump diode at the proper times (t_1 and t_2). The timing diagram for the system can be depicted as in **Figure 3**a, also in Figure 3b the output pulse shape and the transmission function of the (AOM or EOM) modulator are displayed. Note that the depicted components for gain-switching (BS, PD, and diode driver) are symbolic and there are several possible methods to synchronize the pump diode on/off process with the desired times (t_1 and t_2).

In Section 1, we introduced the split pulse generation and MPP due to system dynamics and the situation would be more complicated under the effects of nonlinear scattering phenomena such as SBS and SRS[6,16,17] that can completely distort or split the output pulses in AQS-FLs. Shortening the fiber length and choosing a larger fiber diameter are the common methods for mitigating the above nonlinear effects,[15] however for single mode operation and producing sufficient pulse energy, two contradictory conditions must be met; the fiber core diameter cannot be very large for achieving a single mode operation and the fiber length is required to be above a minimum to provide enough ions and produce the desired pulse energy. These two requirements that limit the effectiveness of the above-mentioned conventional solutions. Another method for mitigating the SBS is phase modulating (chirping) the pump source,[18,19] however this solution is more applicable to the communication transmission systems and passive fibers rather than an AQS-FL system in which the pumping effect would be indirect. Two other effective methods are: i) increasing the laser linewidth and ii) decreasing the output pulse duration.[20] Increasing the laser linewidth effectively reduces the Brillouin gain (g_B) because g_B is inversely proportional to the laser linewidth according to ref. [15]

$$g_B = g_0 \frac{\Delta\nu_B}{\Delta\nu_L + \Delta\nu_B} \tag{1}$$

where g_0 is the Brillouin gain coefficient (BGC) of the host material with a typical value of 5×10^{-11} m W^{-1},[10] $\Delta\nu_B$ is the Brillouin bandwidth in the range of tens of megahertz,[10] and $\Delta\nu_L$ is the laser linewidth, which is in the range of few gigahertz for narrow linewidth fiber lasers.[20]

If having a narrow linewidth laser is not critical, this solution will greatly decrease the SBS effect, although in case of requiring a narrow linewidth, one can examine the shortening of the output pulse duration; if the output pulse duration is short enough, the acoustic modes arising from SBS cannot find adequate time for emergence and growth. Under these conditions the Stokes powers experience an effective mitigation. Unfortunately reducing the timing parameters of the EOM or AOM modulator

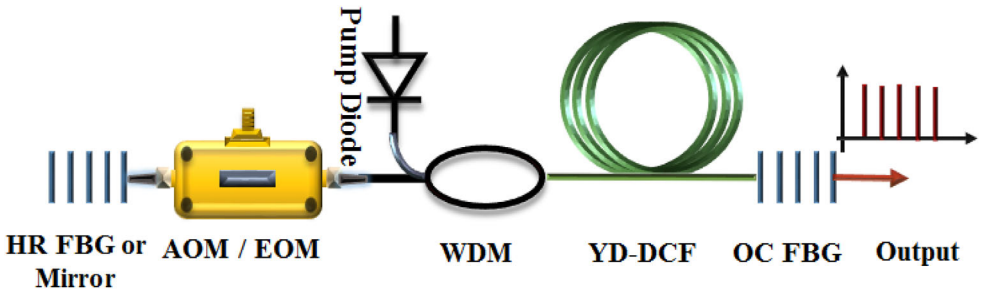

Figure 2. Schematic of the AQS-FL system featuring a simple beam sampler and driver circuitry to turn on (off) the pump diode on the desired times. The components from left to right are high reflectivity fiber Bragg grating (FBG), EOM or AOM modulator, pump diode, WDM coupler, active fiber, pump driver circuit, output coupler (FBG), beam sampler (BS), and photo-detector (PD).

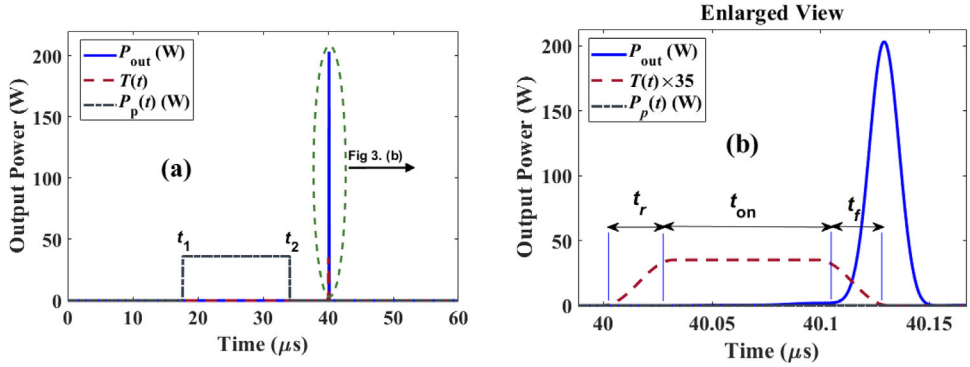

Figure 3. a) Illustration of the output pulse, pump power modulation function $P_p(t)$ and on/off times t_1 and t_2, b) enlarged illustration of the output pulse and modulator transmission function $T(t)$.

particularly its rise time (t_r), in order to reduce the output pulse duration, strongly perturbs the cavity[4] and an irregular pulse shape would be produced that may even further increase the SBS. One can chose a lower core diameter[5] and shorter fiber to produce a shorter pulse; however, this solution may lead to significant decrease of the system deliverable energy on the output because the total cavity volume (hence the number of ions) is reduced. A helpful aspect of producing high peak power pulses is that they demand a high level of storage energy, meaning that a considerable gain must be available along the fiber prior to pulse inception. This large amount of gain, in turn, helps the rapid growth of the pulse, which naturally results in a high peak power and short pulse duration as the system available gain would be rapidly consumed. In fact, contrary to usual criteria, a high peak power pulse may excite lower SBS Stokes power. In spite of this description, for a pulse width of a few ns, a situation may arise that allows very rapid growth of SBS Stokes waves, according to the power evolution equation of SBS Stokes, some amount of power will be transferred from the main pulse to the Stokes waves. This transferred power per unit length of the fiber can be defined utilizing one the following equations[16,17,21]

$$\frac{dP_s}{dz} = -\frac{g_{B(R)}}{A} P_s P_{B(R)} \tag{2}$$

$$\frac{dP_s}{dz} = -\frac{g_B}{A} P_s \rho \tag{3}$$

where P_s and $P_{B(R)}$ are respectively the lasing and Brillouin (Raman) Stokes powers, $g_{B(R)}$ is the Brillouin (Raman) gain and A is the core cross sectional area. Equation (3) is only applicable to SBS and ρ in our modeling method would be the acoustic power of hyper-sound waves induced by SBS or thermal noise. In the next sections, we will use the Equations (2) and (3) to model and describe the SRS and SBS processes respectively. Both of the above equations include the multiplication of two power variables, which may lead to very rapid exponential growth, in this case most of the power (and available gain) will be dedicated to the Stokes components, therefore having a pulse width of a few nanoseconds is not always adequate to suppress the SBS effect. The key point here is finding a state of the system that allows the growth of the main lasing signal over SBS or SRS Stokes orders. The delay between the main pulse and Stokes pulses can be exploited for allowing the rapid growth of the main pulse, while the main pulse consumes considerable gain, the inversion would be decreased and the RHS term in Equations (2) and (3) remains insignificant. On the other hand, dealing with SRS utilizing this method is even more feasible, SRS Stokes orders experience very small emission cross sections and partial FBG reflections in comparison to the main signal. Hence a controlled level of N_2 population above the transparency level during the initial stage of the pulse formation can effectively prevent the inception of SRS Stokes pulses, thus the N_2 population can be seen as an effective bottleneck to the SRS. Further details of this solution will be discussed in Section 4.

Knowing that there is a small delay between the main and Stokes pulses, if the main pulse consumes enough inversion, the SBS Stokes pulses cannot grow effectively, on the other hand, a remaining level of extractable inversion in the fiber provides a good environment for the emergence of considerable Stokes pulses which can even reach to tens or hundreds of kilowatts peak power. This criterion provides the background concept that leads to the idea of inversion level control during the pulse initial growth. In passive fiber SBS modeling, usually there is a pump power and a Stokes power parameter, however in a fiber laser system the pump is not directly engaged in the SBS process and it has an indirect impact on the nonlinear scattering. What is called a "pump" for passive fiber, is our main lasing pulse here. A basic idea might suggest that a stepwise or Gaussian increase of the pump diode power may harness the process. However because of the complicated system behavior, the results are not so promising and an examination of this basic idea leads to partial SBS mitigation with 0.2 nm linewidth lasing—while, with narrow linewidth of 0.02 nm, this method is not effective at all, thus an artificial intelligence (AI) algorithm appears promising. Controlling the pump diode and modulator at the same time combines the controllability and robustness of both gain switching and Q-switching methods. The AI details can be found in Section 5. The resulting AI generated pulse shape manages the system energy in such a way that complete SBS and SRS suppression would be realizable.

3. The Stimulated Brillouin Scattering (SBS)

Thermal noise causes vibrations of the host material that is described by acoustic phonons and spontaneous Brillouin scattering (SpBS). These acoustic vibrations can dramatically escalate due to the intensity of laser beam that eventually leads to SBS; the details can be found in the literature.[18,22,23] The modeling of SpBS and SBS is commonly carried out based on the Gaeta and Boyd model,[23]for example, the modeling method which is utilized in [18]; these models usually describe the long passive fibers for communication systems and opto-mechanical details of the fibers, considering only the propagation equations. The acoustic waves usually are described in these models by material density fluctuations.[18] On the other hand, there are models that describe the acoustic wave by its power, in such models the fiber laser (or amplifier) population rate equations are taken into consideration and coupled to the propagation equations.[16] This method of modeling is more suitable to properly describe the dynamics and behavior of an AQS-FL, additionally Fotiadi et al. in ref. [24] have used some arrangements for the equation indices to model the higher order acoustic and Stokes waves; such arrangements are utilized in ref. [25]. In this work however, we do not need to inspect many of opto-mechanical properties of the fiber or higher order Stokes, so a partial differential equation (PDE) system will be derived in the following to describe the AQS-FL dynamics. A de facto and intuitive model for fiber lasers using the propagation (evolution) and rate equations,[5] suggests the following set of coupled PDEs together with the boundary conditions (BCs) defined by the reflectivity of the mirrors (or FBGs), transmittance of the AOM (EOM) modulator, and the pump power. Here, ytterbium is the dopant, so two-level modeling of the rate equations is adequate to describe the system. The ASE spectrum is divided into K sections (channels), $k = 1$ represents the main lasing (signal) and higher indices point to the ASE components. All of the k-indexed parameters plus the parameters with λ in the parenthesis are wavelength dependent,

$$\frac{\partial P_{\mathrm{p}}}{\partial z} + \frac{1}{v_{\mathrm{p}}}\frac{\partial P_{\mathrm{p}}}{\partial t} = [g_{\mathrm{p}} - \alpha_{\mathrm{p}}]P_{\mathrm{p}} \tag{4}$$

$$\pm\frac{\partial \overset{\pm}{P}_k}{\partial z} + \frac{1}{v_k}\frac{\partial \overset{\pm}{P}_k}{\partial t} = [g_k - \alpha_k]\overset{\pm}{P}_k + 2\sigma_e(\lambda_k)N_2\frac{hc^2}{\lambda_k{}^3}\Delta\lambda_k \tag{5}$$

$$\frac{\partial N_2}{\partial t} = \frac{\lambda_{\mathrm{p}}}{hcA_c}g_{\mathrm{p}} \times P_{\mathrm{p}} - \sum_{k=1}^{K}\frac{\lambda_k}{hcA_c}g_k \times \left(\overset{+}{P}_k + \overset{-}{P}_k\right) - \frac{N_2}{\tau} \tag{6}$$

$$N_0 = N_1 + N_2 \tag{7}$$

$$g_{\mathrm{p}} = \Gamma_{\mathrm{p}}[\sigma_e(\lambda_{\mathrm{p}})N_1 - \sigma_a(\lambda_{\mathrm{p}})N_2] \tag{8}$$

$$g_k = \Gamma_k[\sigma_e(\lambda_k)N_2 - \sigma_a(\lambda_k)N_1] \tag{9}$$

$$k = 1, 2, 3, \ldots, K.$$

In the above system of equations P_{p} is the pump power along the fiber, v_{p} and v_k are the phase velocities of the pump and signal, α_{p} and α_k are the fiber (host) linear attenuation coefficients per meter for the pump and signal wavelengths, $P_{kf(b)}$ represents the signal powers travelling in forward and backward directions, g_{p} and g_k are the absorption and gain coefficients for the pump and signal per meter, σ_{e} and σ_{a} are the absorption and emission cross sections of Yb^{3+} ions in pm^2, h is the Planck constant, c is the speed of light in free space, λ_{p} and λ_k are the pump and signal wavelengths, N_0 is the dopant concentration in fiber core, N_1 and N_2 are the populations of the lower and upper states, τ is the upper state life time, Γ_{p} and Γ_k are the unitless pump and signal overlapping factors. The last RHS term in Equation (5) describes the interaction of spontaneous emission with the laser beam, here the normalized Planck emission term over the ASE range is multiplied by a small angle geometrical approximation for the beam[26] and the presence of $\Delta\lambda$ is to consider the division of ASE range to K channels. The parameter values that are used in our simulations can be found in Section 5. In order to perform a complete transient analysis of the SBS impact on the AQS-FL system for the assessment of AQS-FL behavior under this effect, we need to model and evaluate the noise initiation of SBS, emergence and propagation of acoustic modes, and the interplay between the acoustic field, Stokes fields, and the main lasing field. This implies the conversion of the above PDE system to electric field equivalent system and adding the acoustic equation plus a source of thermal white Gaussian noise. Converting the powers (P) to equivalent electric field (E) terms according to ref. [18]

$$P = \zeta|E|^2 \Leftrightarrow E = \sqrt{\frac{P}{\zeta}} \qquad \left(\zeta = \frac{1}{2}nc\epsilon_0 A_c\right) \tag{10}$$

with the n being the refractive index, ϵ_0 the vacuum permittivity, and recalling that the derivative of a function like u^2 is $2uu'$, we divide both sides of Equation (5) by 2ζE which yields

$$\pm\frac{\partial \overset{\pm}{E}_k}{\partial z} + \frac{1}{v_k}\frac{\partial \overset{\pm}{E}_k}{\partial t} = \frac{1}{2}[g_k - \alpha_k]\overset{\pm}{E}_k + \frac{\sigma_e(\lambda_k)N_2}{\zeta\overset{\pm}{E}_k} \times \frac{hc^2}{\lambda_k{}^3}\Delta\lambda_k \tag{11}$$

Since the division of spontaneous term (last RHS term) by E leads to a divide by zero, the initialization of the fields in a proper manner becomes necessary. Improper field initialization during the simulation leads to a different pulse shape and result and the next step would be subtracting the power that is transferred to the Stokes waves according to Equation (3), which leads to

$$\pm\frac{\partial \overset{\pm}{E_k}}{\partial z}+\frac{1}{v_k}\frac{\partial \overset{\pm}{E_k}}{\partial t} = \frac{1}{2}[g_k-\alpha_k]\overset{\pm}{E_k}-\frac{g_B}{2A_{eff}}\overset{\mp}{E_{Bk}}\overset{\pm}{\rho_k}+\frac{\sigma_e(\lambda_k)N_2}{\zeta \overset{\pm}{E_k}}\times\frac{hc^2}{{\lambda_k}^3}\Delta\lambda_k \quad (12)$$

where $E_k^{\pm}$ is the Brillouin Stokes field of the k_{th} ASE channel, g_B is the Brillouin gain that is introduced in Section 2, and ζ is the conversion constant defined in Equation (10), A_{eff} is the interaction area between acoustic and laser (Stokes) field. This area should be carefully modeled in multimode conditions—unlike for single mode lasing, it can be approximated by wavelength dependent beam cross sectional area; further details on evaluating this parameter can be found in ref. [27]. A similar approach can be adopted in order to create the Stokes waves propagation equation as follows,

$$\pm\frac{\partial \overset{\pm}{E_{Bk}}}{\partial z}+\frac{1}{v_k}\frac{\partial \overset{\pm}{E_{Bk}}}{\partial t} = \frac{1}{2}[g_k-\alpha_k]\overset{\pm}{E_{Bk}}+\frac{g_B}{2A_{eff}}\overset{\pm}{E_k}\overset{\mp}{\rho_k}^*+\frac{\sigma_e(\lambda_k)N_2}{\zeta \overset{\pm}{E_{Bk}}}\times\frac{hc^2}{{\lambda_k}^3}\Delta\lambda_k \quad (13)$$

In modeling of the Stokes waves, the conditions are very similar to the main lasing field; since the SBS only causes a very small shift (around 11 GHz) in frequency,[15] the wavelength and similarly all of the wavelength dependent parameters in the model remain almost the same. It should be emphasized that a term for spontaneous emission impact on Stokes components is needed here.[28,29] A quantitative estimation of this impact on the Stokes components can be performed by utilizing an enhancement/reduction factor or coefficient that is multiplied by a spontaneous emission term. This factor can be dependent on a number of other nonlinear phenomena too, such as four wave mixing,[29] thus a proportionality coefficient based on the lab experiments can be fitted to our model and AI algorithm by design to account for the enhancement or reduction of the ASE effect; for instance in Equation (13) we have used a coefficient of unity. Another consideration should be the ASE spectrum, which is omitted in some models and simulations that is in some models only the main lasing wavelength is taken into account when evaluating the Stokes fields. Here, ASE and SpBS have a dramatic effect on each other, in fact the above system of PDEs tells us these are two sources that compete to inject their own seed to the system, therefore discretization and application of ASE spectrum to the numerical model is fundamental to the accuracy of simulations.

Now we can add the other constitutive equations to the system in order to finalize it. To model the acoustic modes in the fiber, a second order ordinary differential equation (ODE) similar to one of Navier–Stokes equations is utilized in the literature and is convertible to a first order ODE considering the slow varying envelope approximation (SVEA),[18] leading to

$$\frac{\partial\rho}{\partial t}+\frac{\Gamma_B}{2}\rho=\frac{\Gamma_B}{2}\overset{\pm}{E_k}\overset{\mp*}{E_B}+f \quad \left(f=\sqrt{\frac{Q}{\mathrm{d}t\mathrm{d}z}}\delta(t-t')\delta(z-z')\right) \quad (14)$$

in which the Gaussian white noise term f is added to model the SpBS, f is delta-correlated in space (z-direction) and time domains, $\mathrm{d}t$ and $\mathrm{d}z$ are the temporal and spatial steps and the square root term is the strength of noise or noise amplitude that is defined based on the random walk theory and Itô calculus,[30] Q (the strength parameter) can be calculated using ref. [16]

$$Q=\frac{K_B T A_{eff}{\Gamma_B}^2 \nu_g}{2g_B\nu_a} \quad (15)$$

where K_B is the Boltzmann constant, T is the temperature, Γ_B is the relaxation rate of the acoustic modes, ν_g is the group velocity, ν_a is the speed of sound in the fiber, which is equal to 5960 m s^{-1},[18] and g_B is the Brillouin gain defined earlier in Section 2.

Adding the pump power propagation Equation (4) and two rate Equations (6) and (7) conclude the coupled PDE system as follows with all of the parameters defined during the derivation of equations above, expect P_{Bk} which can be calculated from the Stokes field using Equation (10). As such we have the following derived equation system,

$$\frac{\partial P_p}{\partial z}+\frac{1}{\nu_p}\frac{\partial P_p}{\partial t}=[g_p-\alpha_p]P_p \quad (16)$$

$$\pm\frac{\partial \overset{\pm}{E_k}}{\partial z}+\frac{1}{v_k}\frac{\partial \overset{\pm}{E_k}}{\partial t} = \frac{1}{2}[g_k-\alpha_k]\overset{\pm}{E_k}-\frac{g_B}{2A_{eff}}\overset{\mp}{E_{Bk}}\overset{\pm}{\rho_k}+\frac{\sigma_e(\lambda_k)N_2}{\zeta \overset{\pm}{E_k}}\times\frac{hc^2}{{\lambda_k}^3}\Delta\lambda_k \quad (17)$$

$$\pm\frac{\partial \overset{\pm}{E_{Bk}}}{\partial z}+\frac{1}{v_k}\frac{\partial \overset{\pm}{E_{Bk}}}{\partial t} = \frac{1}{2}[g_k-\alpha_k]\overset{\pm}{E_{Bk}}+\frac{g_B}{2A_{eff}}\overset{\pm}{E_k}\overset{\mp}{\rho_k}^*+\frac{\sigma_e(\lambda_k)N_2}{\zeta \overset{\pm}{E_{Bk}}}\times\frac{hc^2}{{\lambda_k}^3}\Delta\lambda_k \quad (18)$$

$$\frac{\partial\rho}{\partial t}+\frac{\Gamma_B}{2}\rho=\frac{\Gamma_B}{2}\overset{\pm}{E_k}\overset{\mp*}{E_B}+f \quad (19)$$

$$\frac{\partial N_2}{\partial t}=\frac{\lambda_p}{hcA_c}g_p\times P_p-\sum_{k=1}^{K}\frac{\lambda_k}{hcA_c}g_k\times\left(\overset{+}{P_k}+\overset{-}{P_k}+\overset{+}{P_{Bk}}+\overset{-}{P_{Bk}}\right)-\frac{N_2}{\tau} \quad (20)$$

$$N_0=N_1+N_2 \quad (21)$$

Since we are using a DCF, the interaction between the pump field and acoustic fields is negligible, hence Equation (16) has been left intact without conversion to a field equivalent. The conversion between fields and their equivalent power, and vice versa, can be carried out when needed during simulation. Care should

be exercised to consider the integrity of dimensions in each equation. All of the terms in each equation should have the same dimension, for example looking at Q in Equation (15) points us to the dimension W^2m, and results in consistency with other terms in Equation (19) and hence Equations (17) and (18). Also looking at Equations (17) and (18) one can conclude that the acoustic field (ρ) appears as power in this type of modeling. To impose the BCs on the solutions of Equations (16)–(21) system, we arrange them as follows

$$\overset{+}{P}_{\mathrm{p}}(0) = \eta_{\mathrm{p}} P_{\mathrm{p}}(t) \tag{22}$$

$$\overset{+}{E}_{k}(0,t) = \overset{-}{E}_{k}(0,t)\sqrt{R_{\mathrm{HR}}(\lambda_k)\eta_k}\,T(t) \tag{23}$$

$$\overset{-}{E}_{k}(L,t) = \overset{+}{E}_{k}(L,t)\sqrt{R_{\mathrm{OC}}(\lambda_k)}\eta_{\mathrm{sp}} \tag{24}$$

$$\overset{+}{E}_{\mathrm{Bk}}(0,t) = \overset{-}{E}_{\mathrm{Bk}}(0,t)\sqrt{R_{\mathrm{HR}}(\lambda_k)\eta_k}\,T(t) \tag{25}$$

$$\overset{-}{E}_{\mathrm{Bk}}(L,t) = \overset{+}{E}_{\mathrm{Bk}}(L,t)\sqrt{R_{\mathrm{OC}}(\lambda_k)}\eta_{\mathrm{sp}} \tag{26}$$

$$k = 1, 2, 3, \ldots, K$$

where (according to schematic in Figure 2) $T(t)$ is the time dependent modulator transmission, R_{OC} is the FBG reflectivity, R_{HR} is the left mirror reflectivity, $P_{\mathrm{p}}(t)$ is the time dependent pump power, η_{sp} is the splicing efficiency between the fiber and FBG, η_{p} is the WDM coupler efficiency for the pump wavelength and η_k is the total efficiency for WDM and other probable coupling components (i.e. lenses, etc.) at the lasing wavelength. The utilized values of these BC parameters can be found in Section 6.

Regarding the presence of a coupled stochastic (Langevin) equation, the system falls into the category of Stochastic PDEs[30] and may be solved using an appropriate Monte–Carlo method. We have solved the system of Equations (16)–(21) using a centered-space-forward-time combinational scheme of the finite difference method (CSFT-FDM)[31] that together with the random walk method, results in a suitable and stable Monte– Carlo algorithm.[30] It is worth pointing out that each loop of the FDM algorithm is called a realization in this method. The mentioned algorithm is implemented later in Section 5 to achieve the optimal pulse shape for suppressing the SBS.

4. The Stimulated Raman Scattering (SRS)

A widely used SRS model for fiber lasers[17,29] is considered and improved resulting in the following system of Equations (27)–(31) and utilized to perform the simulations:

$$\frac{\partial P_{\mathrm{p}}}{\partial z} + \frac{1}{v_{\mathrm{p}}}\frac{\partial P_{\mathrm{p}}}{\partial t} = [g_{\mathrm{p}} - \alpha_{\mathrm{p}}]P_{\mathrm{p}} \tag{27}$$

$$\frac{\partial \overset{\pm}{P}_{k}}{\partial z} + \frac{1}{v_{\mathrm{p}}}\frac{\partial \overset{\pm}{P}_{k}}{\partial t} = [g_k - \alpha]\overset{\pm}{P}_{k} - \frac{\lambda_{\mathrm{Rk}}}{\lambda_k}\frac{g_{\mathrm{R}}}{A_{\mathrm{eff}}}\left(\overset{+}{P}_{\mathrm{Rk}} + \overset{-}{P}_{\mathrm{Rk}}\right)\overset{\pm}{P}_{k} + 2\sigma_e(\lambda_k)N_2\frac{hc^2}{\lambda_k^3}\Delta\lambda_k \tag{28}$$

$$\frac{\partial \overset{\pm q}{P}_{\mathrm{Rk}}}{\partial z} + \frac{1}{v_{\mathrm{p}}}\frac{\partial \overset{\pm q}{P}_{\mathrm{Rk}}}{\partial t} = [G_{\mathrm{Rk}} - \alpha_k]\overset{\pm}{P}_{k} + \frac{g_{\mathrm{R}}}{A_{\mathrm{eff}}}\left(\overset{+}{P}_{k} + \overset{-}{P}_{k}\right)\overset{\pm q}{P}_{\mathrm{Rk}} + 2\sigma_{\mathrm{Re}}(\lambda^q_{\mathrm{Rk}})N_2\frac{hc^2}{\lambda^{q\,3}_{\mathrm{Rk}}}\Delta\lambda^q_{\mathrm{Rk}} \tag{29}$$

$$\frac{\partial N_2}{\partial t} = \frac{\lambda_{\mathrm{p}}}{hcA_c}g_{\mathrm{p}} \times P_{\mathrm{p}} - \left[\sum_{k=1}^{K}\frac{\lambda_k}{hcA_k}g_k \times \left(\overset{+}{P}_{k} + \overset{-}{P}_{k}\right) + \sum_{q=1}^{2}\sum_{k=1}^{K}\frac{\lambda^q_{\mathrm{Rk}}}{hcA_{\mathrm{Rk}}}G_{\mathrm{Rk}} \times \left(\overset{+q}{P}_{\mathrm{Rk}} + \overset{-q}{P}_{\mathrm{Rk}}\right) + \frac{N_2}{\tau}\right] \tag{30}$$

$$N_0 = N_1 + N_2 \tag{31}$$

$$k = 1, 2, 3, \ldots, K,\ q = 1, 2, \ldots$$

where P_{Rk} denotes the power of k_{th} Raman wavelength component, the q superscript the Raman Stokes order, λ_{Rk} is the k_{th} Raman shifted channel wavelength and σ_{Re} is the emission cross section corresponding to the Raman shifted wavelengths, the absorption cross section in shifted wavelength range is almost equal to zero, g_{R} denotes the Raman gain and like the case of SBS it is dependent on the SRS bandwidth and laser linewidth, although since there is a very broad Raman shift in silica fibers and according to Equation (32), g_{R} is almost equal to the Raman gain coefficient g_0 which is around 1×10^{-13} m W^{-1} for silica fibers,[15]

$$g_{\mathrm{R}} = g_0\frac{\Delta\nu_{\mathrm{R}}}{\Delta\nu_{\mathrm{L}} + \Delta\nu_{\mathrm{R}}} \cong g_0 \tag{32}$$

All of the other parameters were already defined in Sections 2 and 3. Similar to the SBS PDE system, here there are some plus terms and some minus terms—the plus terms account for the shifting of energy from lower order to the current order and minus terms account for the energy shifting to higher order from the current order. The lowest order of course, is the main lasing pulse (signal) and the minus terms are wavelength dependent because the shift to higher orders is not spectrally local. In fact, there is a considerable red shift of 13 THz during the Raman scattering that should be accounted here, while for SBS the shift is just in the range of gigahertz, so the wavelength dependent ratios are negligible. In most of the cases SRS is considered as a detrimental effect to the fiber laser systems second to SBS. Although the reason of this classification is conventionally considered due to the higher SRS threshold,[10,20] the SBS/SRS threshold is not always the main contributing factor, by contrast, the SBS threshold may be higher in many cases particularly in a pulsed fiber laser system. Furthermore, defining a threshold for these two phenomena principally does not make sense in AQS-FL systems while they show very diverse and irregular behavior. According to different simulations and comparing to the experimental results of other researchers,[16,17,28,29,33–37] we can express that the SBS is a more serious problem in fiber lasers because the red shift caused by SBS is negligible, hence the Stokes modes enjoy almost the same conditions that are provided for the main lasing component. As such, they can be dramatically amplified

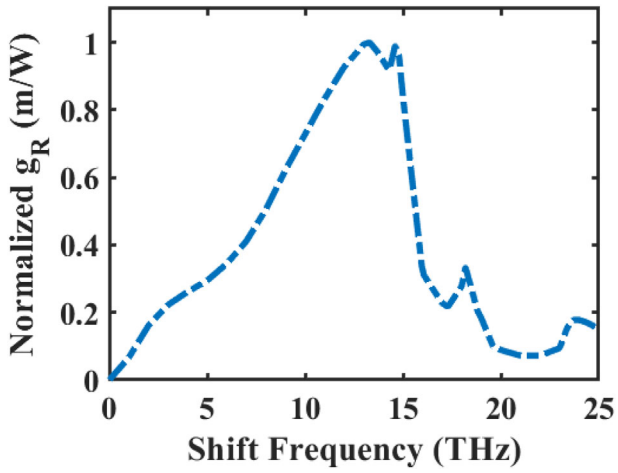

Figure 4. Raman shift spectrum for silica fibers; the spectral data is taken from ref. [40].

to a level that can completely exhaust the energy of the main pulse. Also, SBS strongly perturbs the cavity which is another reason for MPP, additionally in some occasions the pulses are completely separate and irregular. Note that SBS Stokes can reach very high peak power levels that make them catastrophic to the optical fiber. On the other hand, SRS Stokes experiences a very broad shift between 40 to 50 nm for each order. First order SRS Stokes can only partially benefit from the mirror reflections if the mirrors are wavelength selective, for example, FBGs can very effectively reduce the detrimental effects of SRS.[38] Furthermore, if we consider the conventional 70 nm range (1030–1100 nm) for ASE modeling[5,9] and in case of 1080 or 1064 nm lasing, the first order SRS goes beyond 1100 nm, according to extended absorption and emission cross section curves of Yb^{3+} ions,[39] there is a very small emission cross section and almost zero absorption in this range. For the second order SRS, the spectral region is totally out of FBG reflection range and Yb^{3+} emission cross sections can be omitted; so, the above discussion highlights the reasons that make the SRS less detrimental than the SBS in our system.

In our simulations, the Raman gain spectrum of **Figure 4** is considered, additionally the effect of FBGs on the Raman shifted components, the effect of ASE spectral components, and the emission cross sections in the extended range of 1100–1200 nm and the FBG response to the shifted Raman components are taken into account. The Raman Stokes are computed to second order.

5. Genetic Algorithm Development and Implementation

We have developed a multi-objective optimization framework based on the GA that aims at a five-objective goal including peak power, pulse width (FWHM), pulse shape (Gaussian), repetition regime state (attractor),[41] and SBS suppression. The Monte–Carlo method described in Section 3 is implemented in the GA and the chromosomes of algorithm include the Q-switch modulator parameters (t_r, t_f, t_{on}), gain-switching timing parameters (t_1, t_2) and pump power (P_p). Each set of the aforementioned six

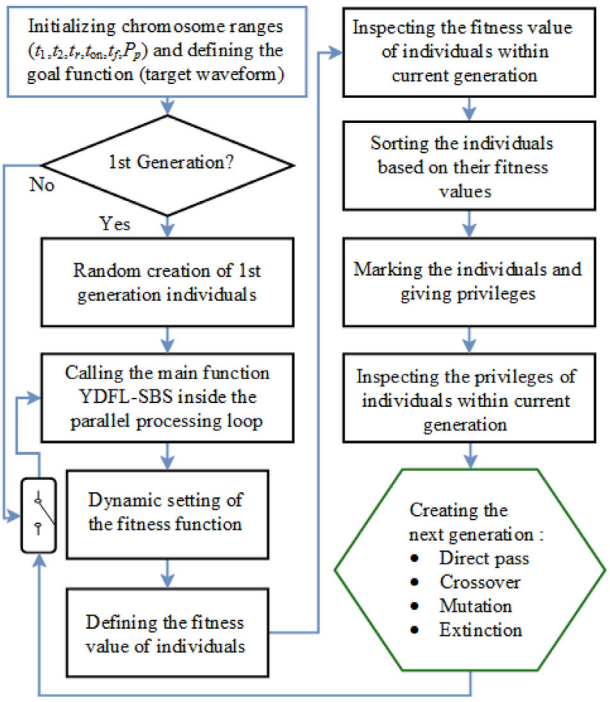

Figure 5. Flowchart of the genetic algorithm.

Table 1. Boundary condition parameters.

Parameter	Description	Value/Range
T	Modulator transmission (Sinusoidal function of time)	0–1
R_{OC}	Output coupler reflectivity	0.25
R_{HR}	High resolution mirror reflectivity	0.995
η_{sp}	Splicing efficiency (Fiber/FBG)	0.98
η_p	WDM coupler efficiency for the pump wavelength	0.85
η_k	Total efficiency for WDM and other probable coupling components (e.g. lenses) at the lasing wavelength	0.65–0.95

parameters specify an individual, and a group of such individuals constitute an evolutionary generation. The GA flowchart is illustrated in **Figure 5**. Further details on the genetic algorithm development and implementation can be found in refs. [9, 42]. Note that the GA must be run after proper fitting of its parameters (chromosomes) and mutation process; exploring the different conditions/ranges, and having the knowledge about the physics of the system is essential. It is considered that GA or other AI algorithms are helpful tools for effectively reducing the time of design for solving inverse problems.[42–45] In case of improper fitting (overfitting or underfitting) the algorithm does not yield the desired results.

6. Simulation Setup and Parameters

We have chosen the following parameters according to the schematic configuration of the Figure 2 and the PDE

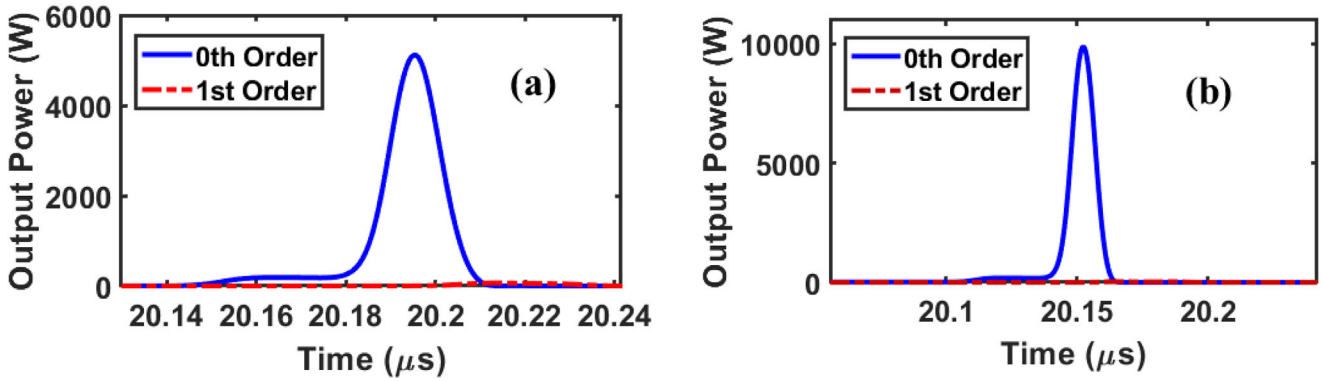

Figure 6. The resulting pulses for the a) 5 kW peak power and b) 10 kW peak power and FWHM of 10 ns in both cases in single pulse operation and based on EOM utilization.

Table 2. The selected ranges for the GA chromosomes.

Parameter	Description	Range
t_1	Pumping start time	0–0.2/f_{sw}
t_2	Pumping stop time	t_1–1/f_{sw}
t_r	Modulator rise time	10–30 [ns]
t_f	Modulator fall time	10–30 [ns]
t_{on}	Modulator on time	10–100 [ns]
P_p	Pump power	20–35 [W]

Table 3. GA results for single and pulse train generation.

Figure	t_r [ns]	t_f [ns]	t_{on} [ns]	P_p [W]	t_1 [ns]	t_2 [ns]
6a	15.93	21.17	160.12	25.34	834	24797
6b	13.45	13.24	120.75	31.80	1858	20295
8a	15.23	15.23	15.01	18.01	2982	16732
8b	15.23	15.23	15.01	18.01	2982	16732

system Equations (16)–(21); a silica YD-DCF of 4 m length, with core/inner cladding diameters of 10/125 μm, Yb^{3+} doping concentration of 5.5×10^{25} m^{-3}, NA equal to 0.06 that leads to single transverse mode of operation, and switching frequency of 40 kHz for the AOM or EOM.[9] The absorption and emission cross sections are taken from refs. [39, 46] and Raman shift is performed according to Figure 4. The Brillouin and Raman gain coefficients for silica fiber are 5×10^{-11} and 1×10^{-13} m W^{-1}[15] and the Brillouin bandwidth is assumed to be 50 MHz.[15] The output FBG is assumed to have 0.25 reflectivity under the lasing wavelength of 1080 nm and pumping is done on the 976 nm wavelength. The pump and signal overlap factors (Γ_p and Γ_k) and loss coefficients (α_p and α_k) are calculated based on the geometry of cylindrical DCF and their wavelength dependency is considered in the model.[47] The spatial step (Δz) is chosen to be 5 cm which provides an appropriate accuracy for the numerical model. Sinusoidal ramp-up and ramp-down is supposed for the modulator transmission function and the values of efficiencies and boundary conditions are specified in **Table 1**. Additionally the chromosome ranges for the single pulse GA are specified

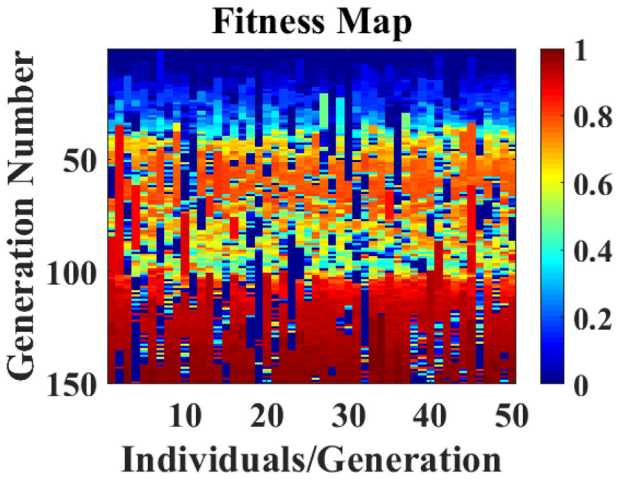

Figure 7. 2D fitness map corresponding to Figure 6b with the color bar indicating the normalized fitness values.

in **Table 2**. The chromosome ranges are selected in such a way to provide suitable fitting, also f_{sw} in Table 2 represents the switching frequency. It is also worth pointing out that a fairly complete set of parameter details for AQS-FL modeling can be found in ref. [9].

7. Results and Discussion

The GA results (the values of six chromosomes) while aiming at 5 and 10 kW peak powers and FWHM equal to 10 ns for single pulse and pulse train generation are shown in **Table 3**. **Figure 6** shows the corresponding pulses for single pulse generation, as can be seen in the figure, the power of Stokes wave is almost zero and the GA has been able to mitigate the SBS effectively. Note that the lasing linewidth in our simulations is supposed to be 0.05 nm that is assumed to be the worst-case scenario; according to Equation (1), having such a narrow linewidth leads to greater Brillouin gain and accordingly the GA is encountered with more difficult conditions.

Figure 7 is the fitness map corresponding to Figure 6b that indicates the GA evolutionary process. The mutations and improvements in generations are obvious through the areas with

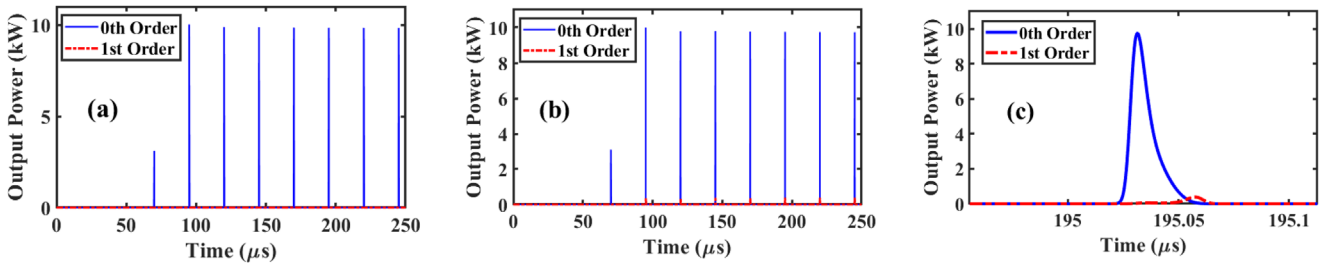

Figure 8. Optimization results under the repetition regime with the switching frequency of 40 kHz using the AOM, a) with the linewidth of 0.05 nm, b) with the linewidth of 0.02 nm, and c) one of the pulses in pulse train (b) is illustrated together with the first order Stokes pulse.

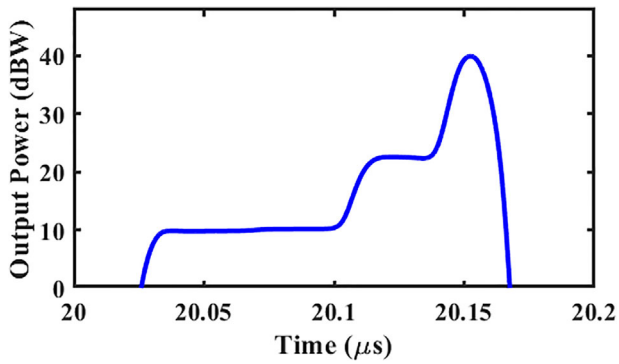

Figure 9. Logarithmic display of the output pulse shape corresponding to Figure 6b.

high level of fitness variation, these areas constitute a horizontal color frontier usually when the GA is properly fitted. The fitness map shows that the GA has the ability to escape from the local optima when looking at the area between 80 and 100 generations, choosing a proper mutation rate is one reason for this successful performance. **Figure 8** demonstrates the GA result for the repetition regime of AQS-FL under the switching frequency of 40 kHz using the AOM, aiming at 10 kW peak power and pulse width of 10 ns. In Figure 8a the linewidth is set to 0.05 nm and the Stokes component totally vanishes while for Figure 8b the linewidth is 0.02 nm and the Stokes component is not totally eliminated. Figure 8c displays one of the pulses corresponding to Figure 8b. The GA takes around 48 h on a 4 core Core i5 and 12 h on a 16 core Threadripper PC for this optimization run and the essential number of generations surprisingly was lower in comparison to the single pulse optimization that is, only 50 generations were needed to reach the results of Figure 8.

A stepwise increase is observable in all of the generated pulse shapes in the above figures, in order to illustrate the pulse shape in detail, a log scale display of Figure 6b is redrawn in **Figure 9** that properly depicts the combination of stepwise and exponential pulse growth. This combination of pulse growth (temporal behavior) leads to very effective suppression of SBS. While it is nearly impossible to manually find such a temporal profile by analytical or trial-error methods, the GA is able to find the desirable temporal profile utilizing the robust and flexible method of combined gain and Q-switching. The initial variations in Figure 9 show that it is almost impossible to find the proper pulse shape by trial and error or classical methods and this is why utilizing the GA is beneficial.

Now let us examine the six GA generated parameters, for example the corresponding result to Figure 6b in our SRS numerical model that was introduced in Section 4; **Figure 10** illustrates the SRS simulation results with the chromosomes corresponding to Figure 6b, by looking at the Figure 10a, a considerable Stokes pulse with the peak power of around 2 kW is observable while we have already predicted that by the effective suppression of SBS, the SRS also should be eliminated and no SRS Stokes pulse should be observed. However by examining the spectrum of the Stokes pulse that is depicted in Figure 10b, it is obvious that the wavelength of this Stokes component is 1080 nm which is the same as in the main lasing process. In Section 4, we had modeled the effect of ASE in our numerical PDE system for SRS simulation and in fact, here we are observing the wavelength components around 1035 nm that are red shifted to 1080 nm by SRS. As a result we must depict and illustrate the sum of both pulses because they are from the same wavelengths. Figure 10c shows the sum result that is consistent with the pulse shape and specifications that we had achieved in Figure 6b when suppressing the SBS. As such, as it was predicted and explained before in Sections 2 and 4, because of the bottleneck created by N_2 population and other limiting factors for the SRS Stokes such as low FBG reflection and very small absorption/emission cross sections, no SRS is observed with this pulse shape and SRS is even more effectively suppressed than SBS.

Another point is that the observable initial tail during the initial stages of the pulse growth in the Figures 6, 9, and 10, is a key contributor to the SBS suppression here; since the SBS is a self-induced process and according to Equations (2), (3), and (18), a rapid growth of the main lasing pulse leads to very rapid exponential growth of the Stokes pulse. On the other hand, a slow growth of the main pulse (regarding the phonon lifetime of the host material) offers the Stokes pulse adequate time and opportunity to use the unconsumed stored energy (available gain) of the fiber.[41,48] As such, the designer should find an intermediate solution while the stepwise and exponential nature of the AQS-FL is considered; here the developed GA finds this middle solution for designers which includes the described initial tail. Additionally we should note that the stepwise or multi-peak behavior occurs when the modulator rise time (t_r) is smaller than the cavity round trip time,[3] examining our GA for example for 2 kW peak power and FWHM of 60 ns with the same fiber length (4 m) showed that the effectiveness of the proposed method is decreased and the GA could eliminate the SBS with the linewidth of 0.1 nm (instead of 0.05 nm) because the system cannot generate the essential stepwise tail, thus one should consider a longer fiber length

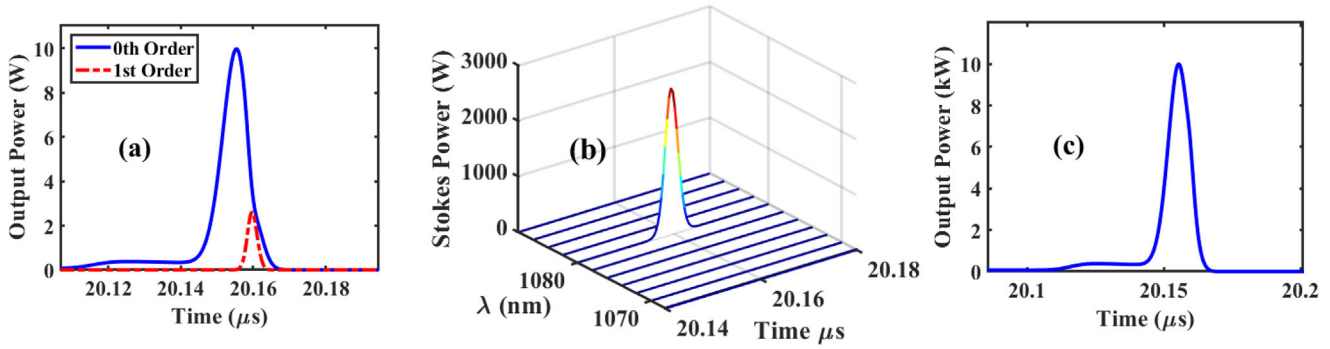

Figure 10. SRS simulation result corresponding to the chromosomes of Figure 6b, a) main and Stokes pulse b) the waterfall diagram for Stokes pulse c) sum of the main and Stokes pulses.

or shorter rise time in order to boost the effect of the proposed SBS suppression method before executing the proposed GA. It is also necessary to explain that the above measure would not lead to MPP, which is a result of the proposed gain and Q-switching combination, in fact using the proposed framework we can generate any sub round-trip Gaussian pulse even within the lower peak power ranges.

7.1. The Feasibility of the Proposed Method

The AOM/EOM modulator limitations are considered in the proposed framework,[9] additionally we have utilized the exponential nature of the fiber lasers and the inherent stepwise tendency of the AQS-FLs. As such, the proposed method just takes advantage of the system behavior and does not try to alter the system nature. On the other hand, according to Figure 3, for the simple gain-switching idea, the pump on/off times (t_1 and t_2) are lying out of the modulator activity time frame. Therefore, the spikes and relaxation oscillations of the fiber cavity or initial instabilities of the pump diode do not interfere with the Q-switching process. Furthermore the pump on/off mechanism can be carried out using a couple of different methods and the schematic of Figure 2, does not strictly recommend the simple gain-switching realization; in fact just realizing the desired t_1 and t_2 parameters matters, for example a modulator controller device featuring the pump diode driver/controller can perform this task. Note that the system is tolerable against the slight variations of the GA result parameters for example, regarding the first row of Table 3, it is not necessary to have the precise modulator rise time of 15.93 ns; a small change in the timings just creates a small change in the output pulse specifications, additionally as mentioned earlier, utilizing a second GA run, one can chose a practical (commercially available) value for the rise time (for instance 15 ns) and run the GA for the second time; further details can be found in ref. [9].

8. Conclusion

In conclusion, we have considered the dynamics of the AQS-FL system in order to exploit its temporal behavior and effectively suppress the SBS. We have considered particularly the stepwise behavior of AQS-FL to manage the stored/consumed energy (hence gain) in the fiber in such a way that most of the energy is dedicated to the growth of the main lasing pulse and almost no energy (gain) remains for the SBS Stokes components. For achieving this goal, we have developed and utilized an innovative multi-objective genetic algorithm (GA) to train the system a temporal behavior that excites the minimum acoustic and therefore the minimum Stokes power. The developed genetic algorithm uses a numerical model for transient SpBS and SBS simulation which we have improved over the previous models, theoretical background, and experiments from other researchers. Additionally, we have improved a conventional numerical model for SRS simulation to form our SRS PDE system. A combinational forward time centered space FDM scheme is utilized for this work and for the stochastic SBS PDE system we have utilized one of the Monte–Carlo methods alongside the aforementioned FDM scheme.

For improved robustness and control over the behavior of the system we have combined the gain switching technique in its simple (on/off) form to activate/deactivate the pumping diode on the proper times. Six chromosomes considered for the GA are including the pump turn on time (t_1), pump turn off time (t_2) in addition to the rise time (t_r), fall time (t_f), and on time (t_{on}) of the modulator plus the pump power (P_p), these six parameters are then found using the GA as a solution to an inverse problem. The optimizations in this work are performed both in single pulse and repetition regimes of AQS-FL and we have used both EOM and AOM to demonstrate the capabilities and feasibility of our proposed algorithm. We theoretically predict that the results of the GA also will cause an effective SRS suppression, as such the resulting parameters from the GA were set into an improved SRS numerical model to examine if the predicted SRS suppression is realizable and the answer was consistent with our theoretical prediction. Furthermore, the resulting pulses from the GA show a temporal tail that is the effective tool in our SBS suppression, this tail can be realized if we set a smaller modulator rise time in comparison to the cavity round-trip time. Using the above-mentioned framework and method, we can achieve 5 and 10 kW peak power and 10 ns wide pulses under the single transverse mode of operation in a 4 m LMA 10/125 YD-DCF silica fiber while a narrow linewidth of 0.05 nm is assumed in the simulations as a worst-case scenario. Under the above conditions, the peak powers of SBS and SRS Stokes waves are negligible. Our proposed framework and method offers the potential for optimized utilization of

different fiber types either for single mode or multi-mode operation over higher power ranges.

Conflict of Interest

The authors declare no conflict of interest.

Data Availability Statement

Research data are not shared.

Keywords

genetic algorithm, Q-switching, stimulated Brillouin scattering; stimulated Raman scattering, suppression

Received: November 6, 2020
Revised: May 8, 2021
Published online:

[1] F. Wang, *JOSA B* **2018**, *35*, 231.
[2] M. C. Falconi, D. Laneve, M. Bozzetti, T. T. Fernandez, G. Galzerano, F. Prudenzano, *J. Lightwave Technol.* **2018**, *36*, 5327.
[3] L. Escalante-Zarate, Y. O. Barmenkov, S. A. Kolpakov, J. L. Cruz, M. V. Andrés, *Opt. Express* **2012**, *20*, 4397.
[4] Y. Wang, C.-Q. Xu, *IEEE J. Quantum Electron.* **2004**, *40*, 1583.
[5] Y. Wang, C.-Q. Xu, *Appl. Opt.* **2006**, *45*, 2058.
[6] B. N. Upadhyaya, A. Kumar, U. Chakravarty, S. M. Oak, M. R. Shenoy, K. Thyagarajan, *IEEE J. Quantum Electron.* **2011**, *47*, 786.
[7] P. Roy, D. Pagnoux, *Opt. Fiber Technol.* **1996**, *2*, 235.
[8] O. G. Okhotnikov, J. R. Salcedo, *Opt. Lett.* **1995**, *20*, 887.
[9] S. Jafari, D. Fathi, H. Taleb, *IEEE Access* **2020**, *8*, 77716.
[10] G. Agrawal, *Nonlinear Fiber Optics*, 5th ed. Academic Press, Cambridge, MA **2013**.
[11] S. Sujecki, *Appl. Sci.* **2018**, *8*, 803.
[12] S. Lamrini, K. Scholle, M. Schäfer, J. Ward, M. Francis, M. Farries, S. Sujecki, T. Benson, A. Seddon, A. Oladeji, B. Napier, P. Fuhrberg, *The European Conf. on Lasers and Electro-Optics*, Optical Society of America, Washington, D.C., **2015**, CJ-7-2.
[13] M. N. Zervas, C. A. Codemard, *IEEE J. Sel. Top. Quantum Electron.* **2014**, *20*, 219.
[14] M. N. Zervas, *Int. J. Mod. Phys. B* **2014**, *28*, 1442009.
[15] P. D. Dragic, M. Cavillon, J. Ballato, *Appl. Phys. Rev.* **2018**, *5*, 041301.
[16] Y. Wang, C.-Q. Xu, *Proc. SPIE* **2006**, *6343*, 63430W.
[17] Y. Wang, C.-Q. Xu, *Proc. SPIE* **2006**, *6343*, 634310.
[18] C. E. Mungan, S. D. Rogers, N. Satyan, J. O. White, *IEEE J. Quantum Electron.* **2012**, *48*, 1542.
[19] C. Zeringue, I. Dajani, S. Naderi, G. T. Moore, C. Robin, *Opt. Express* **2012**, *20*, 21196.
[20] V. V. Ter-Mikirtychev, *Fundamentals of Fiber Lasers and Fiber Amplifiers*, Springer, Cham, Switzerland **2014**.
[21] M. Ferreira, *Electron. Lett.* **1995**, *31*, 1182.
[22] R. W. Boyd, K. Rzaewski, P. Narum, *Phys. Rev. A* **1990**, *42*, 5514.
[23] A. L. Gaeta, R. W. Boyd, *Phys. Rev. A* **1991**, *44*, 3205.
[24] A. A. Fotiadi, G. Ravet, P. Mégret, M. Blondel, *Proc. SPIE* **2004**, *5480*, 71.
[25] L. Pan, I. Utkin, R. Lan, Y. Godwal, R. Fedosejevs, *Opt. Lett.* **2010**, *35*, 895.
[26] B. Sanguinetti, T. Guerreiro, F. Monteiro, N. Gisin, H. Zbinden, *Phys. Rev. A* **2012**, *86*, 062110.
[27] A. Kobyakov, M. Sauer, D. Chowdhury, *Adv. Opt. Photonics* **2010**, *2*, 1.
[28] S. Hou, Y. Lou, N. Zhao, P. Chen, F. Zhang, Y. Chen, F. Lin, J. Li, L. Yang, J. Peng, H. Li, N. Dai, *Opt. Express* **2019**, *27*, 5745.
[29] Z. Zhang, X. Zhou, Z. Sui, J. Wang, H. Li, Y. Liu, Y. Liu, *Opt. Commun.* **2009**, *282*, 1186.
[30] D. J. Higham, *SIAM Rev.* **2001**, *43*, 525.
[31] M. A. Dansson, S. W. Moore, D. B. Soh, R. P. Bambha, Large Core Highly Doped Fiber Amplifiers, SAND2012-8979, Sandia National Laboratories, **2012**, https://doi.org/10.2172/1055880.
[32] M. Karow, J. Neumann, D. Kracht, P. Weßels, *Opt. Express* **2012**, *20*, 10572.
[33] H. Al-Asadi, M. Al-Mansoori, S. Hitam, M. Saripan, M. Mahdi, *Opt. Express* **2011**, *19*, 1842.
[34] M. Abdollahi, M. B. Harouni, M. J. Hekmat, M. Fakhari, N. Shahriari, M. Kanani, H. Normohamadi, *Proc. SPIE* **2016**, *10029*, 182.
[35] V. I. Kovalev, R. G. Harrison, *Opt. Express* **2007**, *15*, 17625.
[36] M. Hekmat, M. Dashtabi, S. Manavi, E. Hassanpour, R. Massudi, *Laser Phys.* **2012**, *23*, 025104.
[37] R. Parvizi, *Int. J. Opt. Photonics* **2013**, *7*, 31.
[38] C.-H. Liu, A. Galvanauskas, V. Khitrov, B. Samson, U. Manyam, K. Tankala, D. Machewirth, S. Heinemann, *Opt. Lett.* **2006**, *31*, 17.
[39] J. W. Dawson, M. J. Messerly, R. J. Beach, M. Y. Shverdin, E. A. Stappaerts, A. K. Sridharan, P. H. Pax, J. E. Heebner, C. W. Siders, C. P. J. Barty, *Opt. Express* **2008**, *16*, 13240.
[40] Q. Lin, G. P. Agrawal, *Opt. Lett.* **2006**, *31*, 3086.
[41] Y. Barmenkov, A. Kir'yanov, M. Andres, *Eur. Phys. J.: Spec. Top.* **2014**, *223*, 2775.
[42] Y. Rahmat-Samii, , in, *17th Int. Conf. on Applied Electromagnetics and Communications*>, IEEE, Piscataway, NJ **2003**.
[43] R. Woodward, E. Kelleher, *Sci. Rep.* **2016**, *6*, 37616.
[44] R. L. Haupt, D. H. Werner, *Genetic Algorithms in Electromagnetics*, John Wiley & Sons, Hoboken, NJ **2007**.
[45] C. E. Predate, P. Mégret, *Opt. Commun.* **2013**, *294*, 241.
[46] R. Paschotta, J. Nilsson, A. C. Tropper, D. C. Hanna, *IEEE J. Quantum Electron.* **1997**, *33*, 1049.
[47] L. Dong, B. Samson, *Fiber Lasers: Basics, Technology, and Applications*, CRC Press, Boca Raton, FL **2016**.
[48] Y. O. Barmenkov, P. Muniz-Canovas, A. V. Kiryanov, A. Carrascosa, J. L. Cruz, M. V. Andres, *J. Lightwave Technol.* **2020**, *38*, 3751.